Functional expression of $Na_V1.7$ channels in freshly dispersed mouse bronchial smooth muscle cells

Matthews, R. M., Bradley, E., Griffin, C. S., Lim, X. R., Mullins, N. D., Hollywood, M. A., Lundy, F. T., McGarvey, L. P., Sergeant, G. P., & Thornbury, K. D. (2022). Functional expression of $Na_V1.7$ channels in freshly dispersed mouse bronchial smooth muscle cells. *American journal of physiology. Cell physiology*, *323*(3), C749-C762. https://doi.org/10.1152/ajpcell.00011.2022

Published in:
American journal of physiology. Cell physiology

Document Version:
Peer reviewed version

Functional expression of Nav1.7 channels in freshly dispersed mouse bronchial smooth muscle cells

Running head:

Fast sodium channels in bronchial smooth muscle

Authors:

R. Matthews- conception and design of research, data acquisition, data analysis, preparation of figures, approval of final version of manuscript. 0000-0001-6691-3310

E. Bradley- conception and design of research, data acquisition, data analysis, preparation of figures, approval of final version of manuscript. 0000-0002-1650-6933

N.D. Mullins – conception and design of research, interpretation of results, editing manuscript, approval of final version of manuscript. 0000-0002-9247-3723

M.A. Hollywood- conception and design of research, interpretation of results, editing manuscript, approval of final version of manuscript. 0000-0002-5119-0874

F.T. Lundy- design of research, interpretation of results, editing manuscript, approval of final version of manuscript. 0000-0003-3150-1150

L.P. McGarvey - design of research, interpretation of results, editing manuscript, approval of final version of manuscript. 0000-0002-2860-0302

G.P. Sergeant- conception and design of research, interpretation of results, approval of final version of manuscript. 0000-0001-9443-5491

K.D. Thornbury- conception and design of research, data analysis, interpretation of results, writing of draft manuscript, preparation of figures, editing manuscript, approval of final version of manuscript. 0000-0002-0750-0847

Affiliation:

Smooth Muscle Research Centre, Dundalk Institute of Technology, Dundalk, County Louth, Ireland

Corresponding author:

K.D. Thornbury, Smooth Muscle Research Centre, Dundalk Institute of Technology, Dublin Rd., Dundalk, County Louth, Ireland (e-mail: keith.thornbury@dkit.ie, Phone: 00353429372434)

ABSTRACT

Isolated smooth muscle cells (SMC) from mouse bronchus were studied using the whole-cell patch clamp technique at ~21°C. Stepping from -100 mV to -20 mV evoked inward currents of mean amplitude -275 pA. These inactivated (tau=1.1 ms) and were abolished when external Na^+ was substituted with *N*-Methyl-D-glucamine. In current-voltage protocols, current peaked at -10 mV and reversed between +20 and +30 mV. The $V_{1/2}$s of activation and inactivation were -25 & -86 mV, respectively. The current was highly sensitive to block by tetrodotoxin (IC_{50}=1.5 nM) and the $Na_V1.7$ subtype selective blocker, PF-05089771 (IC_{50}=8.6 nM), consistent with $Na_V1.7$ as the underlying pore-forming α subunit. Two $Na_V1.7$-selective antibodies caused membrane-delineated staining of isolated SMC, as did a non-selective pan-Na_V antibody. RT-PCR, performed on groups of ~15 isolated SMC, revealed transcripts for $Na_V1.7$ in 7/8 samples. Veratridine (30 μM), a non-selective Na_V channel activator, reduced peak current evoked by depolarization but induced a sustained current of 40 pA. Both effects were readily reversed by tetrodotoxin (100 nM). When veratridine (10 μM) was applied in tension experiments, it induced contractions that were entirely blocked by atropine (1 μM). However, in the presence of atropine, veratridine was able to modulate the pattern of activity induced by a combination of U-46619 & PGE_2, by eliminating bursts in favour of sustained phasic contractions. These effects were readily reversed to control-like activity by tetrodotoxin (100 nM). In conclusion, mouse bronchial SMC functionally express $Na_V1.7$ channels that are capable of modulating contractile activity, at least under experimental conditions.

INTRODUCTION

Bronchodilator drugs are a mainstay in the treatment of obstructive airways diseases such as asthma and chronic obstructive pulmonary disease (COPD). The two most commonly used group of compounds are muscarinic receptor antagonists and adrenergic β receptor agonists, both of which work by causing relaxation of airway smooth muscle cells (ASMC), hence reducing airways resistance and facilitating airflow into the lungs (1). Despite their success, these drugs fail to prevent acute exacerbations of these disorders, which often require hospitalization (2). Furthermore, underdosing due to capped metered doses in inhalers because of safety concerns (3), and loss of broncho-protection with prolonged use, have led to the continued interest in developing novel bronchodilators (1, 4).

One approach to solving this problem is to target other pathways involved in regulating contraction of ASMC. Similar to vascular smooth muscles, ASMC possess an extensive complement of plasmalemmal ion channels, including voltage-dependent Ca^{2+} channels (VDCC, both L- and T-type), K_v7 channels (5), large conductance Ca^{2+}-activated K^+ channels (BK_{Ca}), Ca^{2+}-activated Cl^- channels (Cl_{Ca}) and a variety of TRP channels (6). While in vascular smooth muscle there is little doubt that membrane depolarization, with concurrent influx of Ca^{2+} via L-type Ca^{2+} channels, is an important regulator of vascular tone, in airways smooth muscle this mechanism remains controversial, despite the fact that all of the necessary elements are present (7). However, other studies suggest that membrane potential is an important factor in regulating airways tone, at least in some circumstances. Thus, in $TMEM16A^{-/-}$ mice, there was a significant reduction in bronchial contractile responses to both 5-HT and U-46619 (8), while in mouse and rabbit bronchi potent BK_{Ca} openers inhibited contractions to U-46619 and carbachol (9). Evidence that K_v7 channels might be important in human small airways was also provided by showing that flupirtine (a K_v7 opener) antagonized histamine-induced contractions, while XE991 (a K_v7 blocker) caused severe bronchospasm (5). It is important, therefore, to continue to investigate which plasmalemmal ions channels are present in ASMC and to elucidate their functional contribution to bronchial tone.

In a previous study, we demonstrated that $Na_V1.5$ voltage-dependent sodium channels are expressed in rabbit ASMC (10). So far, this is the only report of Na_V currents in freshly dispersed ASMC, though there are several reports of them in cultured human ASMC (11–13). We have now characterized a Na_V current in freshly dispersed mouse bronchial smooth muscle

cells and examined the effects of activating it with veratridine on isometric tension in bronchial rings. Interestingly, TTX-sensitivity and Na_V channel subtype are markedly different to the current we reported for rabbit but are similar to the Na_V channels and TTX-sensitivity in human cultured ASMC (12).

METHODS

Tissue dissection and cell isolation

All procedures were carried out in accordance with current EU legislation and with the approval of Dundalk Institute of Technology Animal Use and Care Committee. Male and female C57BL/6 mice (10-16 weeks old) were humanely killed by intraperitoneal injection of pentobarbitone and the lungs removed and placed in oxygenated Krebs solution (Solution B). The bronchial tree was exposed by sharp dissection under a microscope to remove surrounding blood vessels and lung tissue. The primary bronchi were removed and cut into small pieces and placed in Hanks Ca^{2+}-free solution (Solution A).

Single airway smooth muscle cells (ASMC) were isolated using a collagenase/proteinase mixture consisting of (per 5 mL of Hanks Ca^{2+}-free solution): collagenase 15 mg (Sigma type 1a), proteinase 1 mg (Sigma type XXIV), BSA 10 mg (Sigma) and trypsin inhibitor 10 mg (Sigma) for approximately 5 min at 37˚C. They were then placed in Hanks Ca^{2+}-free solution (Solution A) and stirred for a further 10 to 20 min to release single relaxed smooth muscle cells. These were plated in Petri dishes containing Hanks Ca^{2+}-free solution (with Ca^{2+} added to a concentration of 100 μM) and stored at 4˚C for use within 6 hours.

Whole Cell Perforated Patch Clamp Recordings

Patch clamp recordings were made using the whole-cell patch clamp configuration patch method as described previously (10). Voltage clamp commands were delivered via an Axopatch 1D patch clamp amplifier (Molecular Devices, Sunnyvale, CA, USA) connected to a Digidata 1322A AD/DA converter (Axon Instruments) interfaced to a computer running pClamp software (Axon Instruments). Pipette solution used in whole cell experiments was rich in Cs^{+} to block K^{+} currents (Solution C). During experiments, the dish containing the cells was superfused with Hanks solution (Solution D). In addition, the cell under study was continuously superfused (Solution D) by means of a close delivery system consisting of a pipette (tip diameter 200 μm) placed approximately 300 μm away. This could be switched, with a dead-space time of <5 s, to a solution containing a drug. In experiments described in Fig. 1*A* and *B*, the superfusion solution was switched from Solution D to Solution E (low Na^{+} Hanks). All patch clamp experiments were carried out at room temperature.

Reverse Transcription (RT-PCR)

RT-PCR was performed on isolated smooth muscle cells and on dissected samples of whole tissue (mouse primary bronchus, mouse brain). In tissue experiments each sample was prepared by pooling bronchial tissue from two same sex and age mice and total RNA were extracted using the TRIzol method (ThermoFisher). For freshly dispersed cells, approximately 15 ASMC were collected from one animal per sample using a micropipette and RNA isolated from using the RNeasy Micro Kit (QIAGEN). All RNA samples were DNase treated to remove any contaminating genomic DNA (DNase 1; ThermoFisher) and then stored at -80ºC for later use. First-strand cDNA was prepared from RNA preparations using the Superscript II Reverse Transcriptase kit (ThermoFisher) as per manufacturer's instructions. End-point PCR was performed on a Techne–Quantica real-time thermal cycler, with Amplitaq Gold PCR Mastermix (Applied Biosystems), using specific custom-designed primers (Table S1). Reactions with brain template cDNA served as positive controls. Reactions without template cDNA served as contamination controls. A second round of 20 PCR cycles was often necessary for the visualization of amplicons from cDNA obtained from isolated cells. In this case, the original PCR product was used in place of the cDNA template. In such cases, the non-template control reaction from the first amplification was also subject to a second amplification process.

Immunocytochemistry

After dispersal, cells were left at room temperature for 90 min to adhere to the bottom of the dish. They were then incubated in 2% paraformaldehyde for 45 min at 4ºC, before being washed three times with 1xDPBS. Cells were then permeabilized with 0.3% Triton X-100, and blocked with donkey serum for 10 minutes, before being washed three times with 1xDPBS. Cells were incubated in anti-Pan Na_V antibody (rabbit polyclonal anti-mouse, 1:200 dilution, Alomone Cat# ASC-003, RRID:AB_2040204), anti-$Na_V1.7$ extracellular epitope (rabbit polyclonal anti-mouse, 1:100 dilution, Alomone Cat# ASC-027, RRID:AB_2341069; the permeabilization step was omitted for this antibody), or anti-$Na_V1.7$ intracellular epitope (rabbit polyclonal anti-mouse, 1:100 dilution, Thermo Fisher Scientific Cat# PA5-77727, RRID:AB_2736575) for 24 hours at 4ºC and then washed three times with 1xDPBS. This was followed by incubation of cells in secondary antibody conjugated to Alexa Fluor™ 488 (donkey polyclonal anti-rabbit antibody, 1:1000 dilution, Molecular Probes Cat# A-21206, RRID:AB_2535792) for 1 hour at 4ºC, and then washed with 1xDPBS for half an hour with a solution change every 5 minutes. Controls were prepared simultaneously. Secondary antibody-

only controls omitted the primary antibody incubation and were processed and imaged with the same parameters as each experimental image. Validation of antibodies: Alomone Cat# ASC-003, RRID:AB_2040204 is widely cited in the literature for neuronal staining (14) and also validated in uterine arteries (15); Alomone Cat# ASC-027, RRID:AB_2341069 was shown to quantitatively stain dorsal root ganglion neurons in a manner consistent with membrane expression of $Na_V1.7$, (16); Thermo Fisher Scientific Cat# PA5-77727, RRID:AB_2736575 has not been cited, but we have independently checked that it stains Chinese hamster ovary (CHO) cells heterologously expressing mouse $Na_V1.7$, but does not cross react with human $Na_V1.5$ expressed in HEK 293 cells (Fig. S1). We have also independently demonstrated that Alomone Cat# ASC-003, RRID:AB_2040204 and Alomone Cat# ASC-027, RRID:AB_2341069 stains $Na_V1.7$ expressing CHO cells in a membrane delineated manner (Fig. S1).

Cells were imaged using an iXon 887 electron multiplying charge coupled device (EMCCD) camera (Andor Technology, Belfast) coupled to a Nipkow spinning disk confocal head (CSU22, Yokogawa, Japan). A 488 nm krypton-argon laser (Melles Griot, UK) was used to excite the Alexa Fluor™ (peak emission 520 nm) conjugated to the secondary antibody bound to the cells. Images were acquired under a x60 objective (Nikon Eclipse Ti) using Andor IQ software. Images were collected at 15 frames per second (FPS) as a stack of TIFFs (pixel size 0.266 x 0.266 μm), prior to analysis in Image J (National Institute of Health, MD, USA).

Isometric tension recordings

Rings, 1-2 mm in length, from primary bronchi were mounted in water-jacketed organ baths, perfused with warmed Krebs solution (Solution B), adjusted to 5 mN tension and allowed to equilibrate for 40 min. Isometric contractions were measured using a Myobath system and data were acquired using DataTrax 2 software (WPI, Hitchin, Hertfordshire, UK). Drugs were delivered by adding them to the organ bath, where they were diluted in Krebs solution to their final concentration.

Drugs & Solutions

The following solutions were used. Concentrations in mM are given in parentheses.

Solution A (Ca^{2+} free Hanks solution for cell dispersal), mM: NaCl (125), KCl (5.4), glucose (10), sucrose (2.9), $NaHCO_3$ (4.2), KH_2PO_4 (0.4), NaH_2PO_4 (0.3), HEPES (10). pH was adjusted to 7.4 using NaOH.

Solution B (Krebs Solution), mM: NaCl (120), KCl (5.9), $NaHCO_3$ (25), $NaH_2PO_4.2H_2O$ (1.2), glucose (5.5), $MgCl_2$ (1.2), $CaCl_2$ (2.5), pH was adjusted to 7.4 by bubbling the solution with 95% O_2 – 5% CO_2 continuously.

Solution C (pipette solution for whole-cell patch clamp recordings), mM: CsCl (133), $MgCl_2.6H_2O$ (1.0), EGTA (2.0), HEPES (10.0), Na_2ATP (1.0), NaGTP (0.1), Na_2 phosphocreatine (2.5), pH adjusted to 7.2 using CsOH.

Solution D (Hanks, bath solution for patch clamp recording), mM: NaCl (125), KCl (5.36), glucose (10), sucrose (2.9), $NaHCO_3$ (4.17), KH_2PO_4 (0.44), NaH_2PO_4 (0.33), $MgCl_2.6H_2O$ (0.5), $CaCl_2.2H_2O$ (1.8), $MgSO_4.7H_2O$ (0.4), HEPES (10), pH adjusted to 7.4 with NaOH.

Solution E (low Na^+ Hanks), mM: *N*-Methyl-D-glucamine (NMDG, 112), NaCl (8.17), KCl (5.36), glucose (10.0), sucrose (2.9), $NaHCO_3$ (4.17), KH_2PO_4 (0.44), NaH_2PO_4 (0.33), $MgCl_2.6H_2O$ (0.5), $CaCl_2.2H_2O$ (1.8), $MgSO_4.7H_2O$ (0.4), HEPES (10.0). pH adjusted to 7.4 using HCl.

Data Analysis and Statistics

All of the experiments in each experimental series were taken from different animals. Hence, 'n' refers both to the number of patches/tissue strips and the number of animals. In each case the gender is noted as (female) or (male). Data were analyzed using Prism software (Graphpad). Summary data are presented as mean ± S.E.M. In voltage clamp experiments, currents were rounded to nearest pA, potentials on curve fits to the nearest mV and time constants (ms) to one decimal place. In concentration-effect curves, IC_{50} values were rounded to two or three significant figures (in nM), as appropriate.

Statistical comparisons were made using either Student's paired test or, if three experimental groups were compared, ANOVA followed by the Tukey *post hoc* test, taking $p < 0.05$ as significant. Data in Fig. 6*E* were compared using the Wilcoxin test for non-parametric data. Statistical test used in each case are noted in the figure legends. For data requiring statistical comparisons (electrophysiology and tension) a minimum sample size of $n = 6$ was chosen, based on previous power calculations and extensive experience. Immunocytochemistry data were not subjected to statistical analysis and were replicated in 3 separate animals.

All experiments employed an *in vitro* within subject (paired samples) experimental model, comparing drug effects with baseline or determining incremental concentration-effect relationships. Randomization was not considered necessary in such experiments. Blinding of the operator was not possible because of the knowledge required to run the experimental

protocols and because responses observed by the operator to manage the experiment permitted inferences about the treatment. Electrophysiological data were analyzed by the operator using pCLAMP software (Molecular Devices) to electronically measure either peak responses found independently by the software or at predetermined time points.

Sigmoidal activation curves were fitted with a Boltzmann equation: $g/g_{max} = 1/\{1 + \exp[\pm(V_{1/2} - V_m)/K]\}$, where $V_{1/2}$ is membrane potential at which there was half-maximal activation, K is the slope factor, V_m is the test potential, g is conductance, and g_{max} is maximal conductance. Conductance (g) was calculated as follows: $g = I/(V_m - E_{Na})$, where E_{Na} is the calculated Nernst potential for Na^+ and I is the current recorded. Inactivation curves were fitted with a similar Boltzmann function: $I/I_{max} = 1/\{1 + \exp[\pm(V_{1/2} - V_c)/K]\}$, where I is the current recorded at the test step, I_{max} is the maximal current recorded, V_c is the conditioning potential (see RESULTS), and K is the slope factor.

Concentration-effect data were fitted with a Hill-Langmuir equation: $I/I_{control} = 1/\{1 + 10\text{^}(\log[\text{Drug}] - \log IC_{50})\}$, where I is the current recorded in the drug, $I_{control}$ is the current in the absence of drug, IC_{50} is the half-maximal effective concentration, and [Drug] is the concentration variable. In each case, IC_{50} is stated, followed by the upper and lower 95% confidence limits (CI, presented in parentheses).

RESULTS

Freshly dispersed ASMC were voltage clamped in the whole cell configuration of the patch clamp technique. Holding at -100 mV and stepping to -20 mV revealed a rapidly inactivating current in ~40% of cells. This current reached its peak within 1-2 ms and rapidly inactivated, with a time constant of 1.1 ± 0.1 ms and mean current amplitude was -275 pA ± 43 pA (n = 15, 8 M, 7 F). The current disappeared when external Na^+ concentration, $[Na^+]_o$, was reduced from 130 to 13 mM (Fig. 1*A* & *B*). This suggests the current was mostly carried by Na^+, hence it will be referred to as I_{Na}. If cells were held at -60 mV and stepped to 0 mV, a slower activating and inactivating, nifedipine-sensitive inward current was sometimes seen. However, under the whole cell recording configuration this usually ran down rapidly and therefore, in most cells, did not interfere with the I_{Na} under study.

Voltage dependence of ASM Na^+ current.

The current-voltage (*I-V*) relationship for I_{Na} was established by holding the cells at -100 mV and then stepping through a range of test potentials from -80 to +50 mV for 100 ms in 10 mV increments. Fig. 1*C* shows representative currents evoked in response to this protocol. The mean *I-V* relationship is shown in Fig. 1*D.* The current activated at potentials positive to -40 mV, peaked at -10 mV and reversed between +20 and +30 mV.

The voltage-dependent inactivation of I_{Na} was examined by holding the cells at a range of conditioning potentials from -120 to +30 mV for 1 s and then stepping to a test potential of -20 mV. Fig. 1*E* shows a representative current response to this protocol where the current inactivated over a voltage range of -100 to -40 mV. A summary of current inactivation and activation in ASMCs is presented in Fig. 1*F* (where activation values are derived from the *I-V* in Fig. 1*D*). Boltzmann fits of these data yielded a $V_{1/2}$ of inactivation of -86 ± 1 mV (slope factor = -9.6), and an activation $V_{1/2}$ of -25 ± 1 mV (slope = 6.8).

Transcriptional expression of Na_V channel subtypes in bronchial tissue and isolated ASMCs.

RT-PCR experiments were performed to determine the transcriptional expression of the Na_V channel α-subtypes in both isolated ASMCs and bronchial tissue. Primer efficacy was initially determined using brain tissue (Fig. 2*A*). All mRNA transcripts encoding the Na_V channel α-subunits were observed in bronchial tissue (Fig. 2*B*). In isolated ASMCs, expression was only observed for a select number of Na_V channel α-subunits. Figure 2*C* presents three examples of Na_V channel expression in different ASMC samples, where it is clear that expression varied from sample to sample. Table 1 summarizes expression in the 8 samples studied, where $Na_V1.7$

was the most consistently expressed subtype (7/8 samples) with $Na_V1.6$ next (4/8) and then $Na_V1.2$ and $Na_V1.9$ (3/8).

Each isolated ASMC mRNA sample was tested for the positive expression of smooth muscle myosin heavy chain (MHC), confirming the presence of ASMCs. In each sample expression of contaminating cell types were also investigated using cell specific markers (UCH-L1 – neuronal cells, CarbA3 – mast cells and P4H – fibroblasts). Primer efficacy for the markers was determined using brain tissue (Fig. 2*D*). All samples in Table 1 had positive expression for MHC and were negative for the other cell markers (Fig. 2*E*).

Pharmacology of ASM Na^+ current

The effect of various pharmacological Na^+ channel modulators were examined on I_{Na}, including some Na_V α-subunit selective blockers, to help determine the phenotype expressed in ASMC.

First, sensitivity to TTX was determined. Na_V subtypes are classified as either TTX-sensitive (IC_{50} in the nanomolar range, $Na_V1.1$, 1.2, 1.3, 1.4, 1.6, & 1.7), TTX-insensitive (IC_{50} = 1–2 μM, $Na_V1.5$) and TTX-resistant (IC_{50} > 40 μM, $Na_V1.8$ & 1.9) (17). Cells were held at -100 mV for 1 s and then stepped to a test potential of -20 mV for 100 ms. TTX reduced current amplitude in a concentration-dependent manner, with 50% inhibition occurring between 1 and 3 nM, e.g. Fig. 3*A*. Summary data for similar experiments are displayed in Fig. 3*B*, where fits of the data with the Hill-Langmuir equation yielded an IC_{50} value of 1.5 nM, 95% CI = 1.2 to 1.8 nM. Hence, the current was TTX-sensitive, excluding $Na_V1.5$, 1.8 or 1.9 as the α-subunits involved.

Next, two subtype-selective blockers were tested for $Na_V1.7$ and $Na_V1.6$, the two most frequent subtypes observed in Table 1. Fig. 3*C* shows an example of the effect of PF-05089771, a $Na_V1.7$ blocker, where the current was concentration-dependently blocked in the nM range. Summary data fitted with the Hill-Langmuir equation, yielded an IC_{50} value of 6.6 nM, 95% CI = 5.1 to 8.6 nM, consistent with the idea that $Na_V1.7$ underlies I_{Na} in mouse ASMC. In contrast, although 4,9-anhydro-TTX blocked the current, it did so with an IC_{50} of 76 nM (95% CI = 67 to 87 nM), considered too high for subtype-selective block of $Na_V1.6$, where the IC_{50} has been reported as 7.8 nM (18). However, we independently checked the sensitivity of mouse $Na_V1.7$ channels overexpressed in CHO cells to 4,9-anhydro-TTX and found that it blocked

these with an IC_{50} (114 nM) in the same order as we found for the current in native ASMC (Fig. S2).

The scorpion toxin, OD1 is a potent activator of $Na_V1.7$, but to a lesser extent other TTX-sensitive currents (19). Fig. 4*A* shows an example of the effect 50 nM of this toxin on the sodium current in an ASMC, where it clearly increased both the current amplitude and the τ of inactivation. Fig. 4*B* is the same experiment as Fig. 4*A*, plotted on a compressed timescale to show the full duration of the sweep (100 ms), where it is clear that OD1 also induced a component of sustained current. Summaries of the effect of OD1 are presented in Fig. 4*C*, where peak current amplitude increased from -222 ± 60 pA to -349 ± 96 pA, and Fig. 4*D*, where sustained current amplitude increased from -17 ± 4 pA to -30 ± 7 pA. In these experiments the τ of inactivation increased from 1.2 ± 0.1 ms to 2.4 ± 0.5 ms ($p = 0.022$, *t*-test).

Effect of veratridine on ASM Na^+ current

The effect of the non-selective Na_V channel activator, veratridine (30 μM) was examined in ASMCs. Veratridine inhibits inactivation of Na^+ channels, resulting in increased Na^+ permeability despite decreased single-channel conductance (20). Consequently, in ASMCs, veratridine caused a reduction in peak current amplitude (Fig. 5*A*) in addition to producing a sustained current (Fig. 5*B*). Peak current amplitude (Fig. 5*C*) was significantly reduced from -153 ± 26 to -91 ± 19 pA, whereas sustained current amplitude (Fig. 5*D*) was increased from -14 ± 6 to -40 ± 7 pA. TTX (100 nM) effectively blocked the current in the presence of veratridine (Fig. 5*A-D*).

Effect of inducing I_{Na} on agonist-induced tension

An attempt was made to assess the functional role of I_{Na} on contractile activity in intact bronchial rings, by examining the effect of modulators of I_{Na}. Veratridine caused a robust contraction that was abolished by atropine (Fig. 6*A* & *B*). This result is easily explained by the fact that veratridine can cause neurotransmitter release by increasing I_{Na} in neurones (21), however, it is noteworthy that when muscarinic receptors were blocked there was no residual direct effect of veratridine. In several other smooth muscle tissues, while veratridine may have no direct contractile effect, it can potentiate the effects of excitatory agonists (for references see Discussion). Therefore, we investigated if this was the case in mouse airway. Because of veratridine's effect on ACh release, it was necessary to have atropine present throughout these experiments, which precluded investigating its effect on cholinergic agonists. Therefore, we

turned our attention to U-46619, a thromboxane analogue. Preliminary experiments showed that veratridine did not potentiate contractures induced by U-46619 (data not shown). However, when PGE_2 was added following application of U-46619, a typical pattern of 'bursts' of phasic contractions occurred (Fig. 6*C*). When veratridine (10 μM) was added to tissues experiencing bursts, the pattern was rapidly changed to a continuous series of phasic contractions, rather than intermittent bursts (Fig. 6*D* & *E*). This pattern continued in all preparations tested throughout the 20 min of veratridine application, however a bursting pattern was restored on application of TTX in the continued presence of veratridine (Fig. 6*D* & *E*). Hence, the modulation of bursting activity by veratridine appears to be due to activation of Na_V channels, rather than an off-target effect. The bursts appeared shorter in duration when TTX was added, therefore we also examined the effect of TTX in the absence of veratridine. The bursts were little affected by TTX, suggesting that Na_V channels were not involved in their formation (Fig. 6*F* & *G*).

Immunological detection of Na_V channel in ASMCs

Based on the sensitivity of the ASM I_{Na} to $Na_V1.7$ modulators, PF-05089771 and OD1, in conjunction with the consistent transcriptional expression of the subtype in isolated ASMCs (Table 1), immunoreactivity to anti-$Na_V1.7$ was examined. ASMCs displayed immunoreactivity to anti-Pan Na_V , a non-α-subunit selective antibody (Alomone ASC-003), with predominant staining concentrated to the periphery of the cell (Fig. 7*A*). Additionally, ASMCs displayed positive expression for $Na_V1.7$ using both an intracellular binding antibody to $Na_V1.7$ (Thermofisher PA5-77727, Fig. 7*B*) and an extracellular binding antibody to $Na_V1.7$ (Alomone ASC-027, Fig. 7*C*). In each case, the cells exhibited distinct membrane-localized immunofluorescent labelling, indicating plasmalemmal expression of $Na_V1.7$ in isolated ASMCs.

A negative control (secondary antibody, no primary antibody incubation) was prepared simultaneously and imaged using the same parameters to ensure no positive immunoreactivity occurred (data not shown).

DISCUSSION

The first report of Na_V currents in airway smooth muscle cells concluded that they were expressed in cultured, but not freshly dispersed human cells (11). Expression also was later confirmed in cultured mouse ASMC (12, 13). However, we subsequently showed that a Na_V current was robustly expressed in freshly dispersed ASMC from rabbit bronchi (10) and also demonstrated that aggressive treatment with enzymes commonly used to disperse cells could abolish the current. The latter finding was similar to that of Berra-Romani in mesenteric arteries, who concluded that Na_V channels could be easily damaged by cell dispersal procedures (22).

We have now characterized a fast Na^+ current in freshly dispersed smooth muscle cells from mouse primary bronchi. This current was nearly 1000-fold more sensitive to TTX compared to the rabbit Na_V current [IC_{50} = 1.1 μM in rabbit, = 1.5 nM in mouse, (10)], suggesting that there are species differences in the underlying Na_V α-subunit isoforms. There are nine known pore conducting Na_V α-subunit isoforms, designated $Na_V1.1$-1.9, that vary in their sensitivity to TTX (17). These are classified as TTX-sensitive ($Na_V1.1$, 1.2, 1.3, 1.4, 1.6 & 1.7, IC_{50} in nanomolar range), TTX-insensitive ($Na_V1.5$, IC_{50} = 1-2 μM) and TTX-resistant (IC_{50} = 40-60 μM; 17.Catterall *et al.*). On this basis, we concluded that the current expressed in rabbit bronchi was mainly mediated by $Na_V1.5$ (10). The TTX-sensitivity of the mouse current suggested that it could belong to any one of $Na_V1.1$-1.4, 1.6 or 1.7. However, it is noteworthy that in human cultured airway myocytes the current was also 'TTX-sensitive' (11, 12) and RT-PCR experiments revealed transcriptional expression of $Na_V1.7$ (12, 13).

We further explored the Na_V isoforms in the mouse ASMC using both pharmacological and molecular approaches. RT-PCR on dispersed cells revealed transcription of $Na_V1.7$ in 7/8 animals (Table 1). High sensitivity to PF-05089771, a $Na_V1.7$ subtype-specific blocker, also supported the idea that $Na_V1.7$ was main subtype underlying the current. This drug blocked the mouse ASMC current with an IC_{50} = 6.6 nM, which is similar to the values found in heterologously expressed $Na_V1.7$ channels from mouse (IC_{50} = 8 nM) and human (IC_{50} = 11 nM), and is 10 to 1000-fold less than the other TTX-sensitive Na_V subtypes (23). The ASMC current was also potentiated by the scorpion toxin, OD1 (50 nM), which is relatively selective for $Na_V1.7$ and $Na_V1.4$ (EC_{50} of 7-10 nM), compared to other Na_V subtypes (EC_{50} ≥ 3 μM), although $Na_V1.6$ has an intermediate sensitivity to it [EC_{50} = 47 nM; (19)]. In RT-PCR

experiments, $Na_V1.6$ transcripts were found in dispersed cells from 4/8 animals, the second highest fraction (Table 1). However, functional expression of $Na_V1.6$ in mouse ASMC was not supported by experiments with 4,9-anhydro-TTX, which has been reported to block mouse $Na_V1.6$ with an IC_{50} of 7.8 nM (18), compared to mouse ASMC (IC_{50} = 76 nM, Fig. 3*F*) and mouse $Na_V1.7$ expressed in CHO cells (IC_{50} = 114 nM, Fig. S2). Transcripts for $Na_V1.1$, 1.2, 1.5 and 1.9 were also found in some RT-PCR samples collected from dispersed ASMC, however, the fact that there was no residual current in the presence of 100 nM PF-05089771, suggests that they contributed little to the net current under the conditions of our experiments. Finally, expression of $Na_V1.7$ protein was confirmed in immunocytochemistry experiments, where two $Na_V1.7$ specific antibodies produced well defined membrane delineated staining of isolated ASMC. Taken together, these data support $Na_V1.7$ as the main subtype underlying the ASMC sodium current, but they do not completely exclude minor contributions from other subtypes.

The physiological relevance of the ASM I_{Na} is puzzling, given its negative inactivation kinetics and narrow window current. Under the conditions of our experiments, the inactivation $V_{1/2}$ of I_{Na} was -86 mV, which is negative, even by the standards of $Na_V1.7$ (17). However, the inactivation $V_{1/2}$ for $Na_V1.7$ can be quite variable, even within the same species and expression system [e.g. -54 mV to -96 mV for human $Na_V1.7$ in HEK 293 cells; (23)], suggesting that this property may be regulated by intracellular control mechanisms. The inactivation $V_{1/2}$ of human $Na_V1.7$ shifted 20 mV to the right when the pore forming α-subunits were co-expressed with regulatory β1-subunits (24). Thus, it is possible that the availability of ASMC I_{Na} could increase under conditions where expression of β1-subunits is increased, or if other regulatory factors come into play. The availability of the current also depends on the resting membrane potential (RMP), but unfortunately, there is limited research into the RMP of ASMC in general, and in particular for the more pathologically relevant, distal airways. Values of -45, -50, -60 and -48 mV have been reported for human, guinea pig, canine and bovine trachea, respectively, though it is unclear if this variation was due to genuine species differences or technical differences in recording (25–27). The RMP of canine 2nd order bronchi was found to be more negative than the RMP recorded in the trachea (26), suggesting that the distal airways may have a more hyperpolarized RMP.

When we examined the potential role of I_{Na} in tension experiments, we found that TTX had no effect on activity induced by U-46619. We therefore attempted to activate I_{Na} in the tissue with

veratridine. Veratridine induced tonic contractions that were abolished by atropine (Fig. 6*A* & *B*), indicating that they were due to acetylcholine release, presumably from nerve endings. In contrast to the experiments on rat mesenteric artery (28), veratridine did not exert any direct effect on the tissue once the effect of neurotransmitter release was blocked. Veratridine also failed to enhance tonic contraction induced by U-46619 alone (data not shown), however, when U-46619 and PGE_2 were applied together, a bursting pattern of phasic contractions emerged that was rapidly modified by veratridine in a TTX-sensitive manner. PGE_2 has been shown to strongly activate large-conductance Ca^{2+}-activated K^+ (BK) channels in mesenteric artery myocytes (29) and hyperpolarizes vas deferens and colonic smooth muscle cells (30, 31). Cyclic AMP, the second messenger associated with inhibitory PGE_2 responses, has also been shown to activate BK channels in airway smooth muscle cells (32). It is therefore possible that hyperpolarization induced by PGE_2 could have unmasked the effect of veratridine by increasing the availability of I_{Na}. While these experiments did not demonstrate a role for I_{Na}, they did indicate that that activation of I_{Na} was capable of inducing changes in tension when the nerves were blocked.

It is reasonable to speculate that the ASMC Na_V current could become up-regulated under inflammatory conditions. Nerve growth factor (NGF) is a potent up-regulator of $Na_V1.7$ channels (33, 34) and is also well known to contribute to airway hyper-responsiveness in inflammatory lung conditions such as asthma and chronic obstructive pulmonary disease [COPD; (35, 36)]. Serum levels of NGF are elevated in COPD, commensurate with the stage of the disease (37) and ASMC constitutively express NGF, increasing dose-dependently in response to the pro-inflammatory cytokine interleukin (IL-1β) (38). Interestingly, $Na_V1.7$ expression increased in bronchi extracted from ovalbumin-sensitized guinea-pig airways and ProTx III, a $Na_V1.7$ blocker, reduced airway resistance under these conditions (39). However, since bronchial parasympathetic nerves also highly express $Na_V1.7$, it is not possible at present to conclude if ASMC $Na_V1.7$ channels contributed to this effect.

Finally, the contention of previous authors that there is preferential expression of Na_V channels in cultured versus freshly dispersed smooth muscle cells, led them to speculate that Na_V appear during de-differentiation and are involved in proliferation and remodeling (12, 13). The fact that we have now shown functional Na_V expression in freshly dispersed ASMC from two different species does not in any way preclude this possibility, therefore involvement in airways remodelling in chronic diseases such as asthma and COPD must remain a consideration.

SUPPLEMENTAL DATA

Supplemental Figures S1 and S2 and Supplemental Table S1. https://doi.org/10.6084/m9.figshare.18285617

ACKNOWLEDGEMENTS

mNaV1.7-CHO (Chinese Hamster Ovary) cells were gifted by École Polytechnique Fédérale de Lausanne (EPFL), Switzerland, in collaboration with The Blue Brain Project. The authors also gratefully acknowledge technical assistance from Mrs Billie McIlveen.

GRANTS

This work was performed as part of the BREATH project, funded by the European Commission Interreg VA Health and Life Science Programme (Grant#: INT-VA/045).

DISCLOSURES

No conflicts of interest, financial or otherwise, are declared by the authors.

AUTHOR CONTRIBUTIONS

R.M and E.B conception and design of research, data acquisition, data analysis, preparation of figures, approval of final version of manuscript. N.D.M, M.A.H and G.P.S. conception and design of research, interpretation of results, editing manuscript, approval of final version of manuscript. F.L and L.P.M design of research, interpretation of results, editing manuscript, approval of final version of manuscript. K.D.T conception and design of research, data analysis, interpretation of results, writing of draft manuscript, preparation of figures, editing manuscript, approval of final version of manuscript.

REFERENCES

1.**Spina D.** Current and novel bronchodilators in respiratory disease. *Curr Opin Pulm Med* 20(1): 73–86, 2014. doi: 10.1097/MCP.0000000000000012.

2.**Wedzicha JA, Seemungal TA.** COPD exacerbations: defining their cause and prevention. *Lancet* 370(9589): 786–96, 2007. doi: 10.1016/S0140-6736(07)61382-8.

3.**Moulton BC, Fryer AD.** Muscarinic receptor antagonists, from folklore to pharmacology; finding drugs that actually work in asthma and COPD. *Br J Pharmacol* 163(1): 44–52, 2011. doi: 10.1111/j.1476-5381.2010.01190.x

4.**Cazzola M, Rogliani P, Matera MG**. The future of bronchodilation: looking for new classes of bronchodilators. *Eur Respir Rev* 28(154): 190095, 2019. doi: 10.1183/16000617.0095-2019.

5.**Brueggemann LI, Kakad PP, Love RB, Solway J, Dowell ML, Cribbs LL, Byron KL.** Kv7 potassium channels in airway smooth muscle cells: signal transduction intermediates and pharmacological targets for bronchodilator therapy. *Am J Physiol Lung Cell Mol Physiol* 302(1): L120–32, 2012. doi: 10.1152/ajplung.00194.2011.

6.**Perez-Zoghbi J, Karner C, Ito S, Shepherd M, Alrashdan Y, Sanderson M.** (2009). Ion channel regulation of intracellular calcium and airway smooth muscle function. *Pulmonary Pharmacology & Therapeutics* 22(5): 388–397, 2009. doi: 10.1016/j.pupt.2008.09.006.

7.**Janssen, L.** Ionic mechanisms and Ca2+ regulation in airway smooth muscle contraction: do the data contradict dogma? *Am J Physiol Lung Cell Mol Physiol* 282(6): L1161–78, 2002. doi: 10.1152/ajplung.00452.2001.

8.**Wang P, Zhao W, Sun J, Tao T, Chen X, Zheng Y, Zhang C, Chen Z, Gao Y, She F, Li Y, Wei L, Lu P, Chen C, Zhou J, Wang D, Chen L, Shi X, Deng L, ZhuGe R, Chen H, Zhu M.** Inflammatory mediators mediate airway smooth muscle contraction through a G protein-coupled receptor–transmembrane protein 16A–voltage-dependent Ca2+ channel axis and contribute to bronchial hyperresponsiveness in asthma. *J Allergy Clin Immunol* 141(4): 1259–1268.e11, 2018. doi: 10.1016/j.jaci.2017.05.053.

9.**Bradley E, Large R, Bihun V, Mullins N, Hollywood M, Sergeant G, Thornbury K.** (2018). Inhibitory effects of openers of large-conductance Ca2+-activated K+ channels on agonist-induced phasic contractions in rabbit and mouse bronchial smooth muscle. *Am J Physiol Cell Physiol* 315(6): C818–29, 2018. doi: 10.1152/ajpcell.00068.2018.

10.**Bradley E, Webb T, Hollywood M, Sergeant G, McHale N, Thornbury K.** The cardiac sodium current Nav1.5 is functionally expressed in rabbit bronchial smooth muscle cells. *Am J Physiol Cell Physiol* 305(4): C427–35, 2013. doi: 10.1152/ajpcell.00034.2013.

11.**Snetkov V, Hirst S, Ward J.** Ion channels in freshly isolated and cultured human bronchial smooth muscle cells. *Exp Physiol* 81(5): 791–804, 1996. doi: 10.1113/expphysiol.1996.sp003977.

12.**Jo T, Nagata T, Imuta H, Ma J, Hara K, Omata M, Nagai R, Takizawa H, Nagase T, Nakajima T.** Voltage-gated sodium channel expressed in cultured human smooth muscle cells: involvement of SCN9A. *FEBS Lett* 567(4): 339–343, 2004. doi: 10.1016/j.febslet.2004.04.092.

13.**Nakajima T, Jo T, Meguro K, Oonuma H, Ma J, Kubota N, Imuta H, Takano H, Iida H, Nagase T, Nagata T.** Effect of dexamethasone on voltage-gated Na+ channel in cultured human bronchial smooth muscle cells. *Life Sci* 82(23-24): 1210–1215, 2008. doi: 10.1016/j.lfs.2008.04.007.

14.**Sobieski C, Jiang X, Crawford DC, Mennerick S.** Loss of Local Astrocyte Support Disrupts Action Potential Propagation and Glutamate Release Synchrony from Unmyelinated Hippocampal Axon Terminals In Vitro. *J Neurosci* 35(31):11105–17, 2015. doi: 10.1523/JNEUROSCI.1289-15.2015.

15.**Virsolvy A, Fort A, Erceau L, Charrabi A, Hayot M, Aimond F, Richard S.** Hypoxic Conditions Promote Rhythmic Contractile Oscillations Mediated by Voltage-Gated Sodium Channels Activation in Human Arteries. *Int J Mol Sci* 22(5): 2570, 2021. doi: 10.3390/ijms22052570.

16.**François-Moutal L, Dustrude ET, Wang Y, Brustovetsky T, Dorame A, Ju W, Moutal A, Perez-Miller S, Brustovetsky N, Gokhale V, Khanna M, Khanna R.** Inhibition of the Ubc9 E2 SUMO-conjugating enzyme-CRMP2 interaction decreases NaV1.7 currents and reverses experimental neuropathic pain. *Pain* 159(10): 2115–2127, 2018. doi: 10.1097/j.pain.0000000000001294.

17.**Catterall W, Goldin A, Waxman S.** International Union of Pharmacology. XLVII. Nomenclature and Structure-Function Relationships of Voltage-Gated Sodium Channels. *Pharmacol Rev*, 57(4): 397–409, 2005. doi: 10.1124/pr.57.4.4.

18.**Rosker C, Lohberger B, Hofer D, Steinecker B, Quasthoff S, Schreibmayer W.** The TTX metabolite 4, 9-anhydro-TTX is a highly specific blocker of the $Na_V1.6$ voltage-dependent sodium channel. *Am J Physiol* 293(2): C783–C789, 2007. doi: 10.1152/ajpcell.00070.2007.

19. **Deuis JR, Mueller A, Israel MR, Vetter I.** The pharmacology of voltage-gated sodium channel activators. *Neuropharmacol* 127: 87–108, 2017. doi: 10.1016/j.neuropharm.2017.04.014.

20.**Wang GK, Wang SY.** Veratridine block of rat skeletal muscle NaV1.4 sodium channels in the inner vestibule. *J Physiol* 548(3): 667–675, 2003. doi: 10.1113/jphysiol.2002.035469. doi: 10.1113/jphysiol.2002.035469.

21.**Massensini A, Romano-Silva M, Gomez M.** Sodium Channel Toxins and Neurotransmitter Release. *Neurochem Res*, 28(10): 1607–1611, 2003. doi: 10.1023/a:1025643030044.

22.**Berra-Romani R, Blaustein MP, Matteson DR.** TTX-sensitive voltage-gated Na+ channels are expressed in mesenteric artery smooth muscle cells. *Am J Physiol Heart Circ Physiol* 289(1): H137–45, 2005. doi: 10.1152/ajpheart.01156.2004.

23.**Alexandrou A, Brown A, Chapman M, Estacion M, Turner J, Mis M, Wilbrey A, Payne E, Gutteridge A, Cox P, Doyle R, Printzenhoff D, Lin Z, Marron B, West C, Swain N, Storer R, Stupple P, Castle N, Hounshell J, Rivara M, Randall A, Dib-Hajj S, Krafte D, Waxman S, Patel M, Butt R, Stevens E.** Subtype-Selective Small Molecule Inhibitors Reveal a Fundamental Role for Nav1.7 in Nociceptor Electrogenesis, Axonal Conduction and Presynaptic Release. *PLOS ONE* 11(4): p.e0152405, 2016. doi:10.1371/journal.pone.0152405.

24. **Klugbauer N, Lacinova L, Flockerzi V, Hofmann F.** Structure and functional expression of a new member of the tetrodotoxin-sensitive voltage-activated sodium channel family from human neuroendocrine cells. *EMBO J* 1995 14(6): 1084–90, 1995. doi: 10.1002/j.1460-2075.1995.tb07091.x.

25.**Honda K, Tomita T.** Electrical activity in isolated human tracheal muscle. *Japan J Physiol* 37(2): 333–336, 1987. doi: 10.2170/jjphysiol.37.333.

26.**Souhrada M, Klein J, Berend N, Souhrada J.** Topographical differences in the physiological response of canine airway smooth muscle. *Respir Physiol* 52(2): 245–258, 1983. doi: 10.1016/0034-5687(83)90009-9.

27.**Kirkpatrick, C**. Excitation and contraction in bovine tracheal smooth muscle. *J Physiol* 244(2): 263–281, 1975. doi: 10.1113/jphysiol.1975.sp010796.

28.**Ho WSV, Davis AJ, Chadha PS, Greenwood IA.** Effective contractile response to voltage-gated Na^+ channels revealed by a channel activator. *Am J Physiol* 304(8): C739–C747, 2013. doi: 10.1152/ajpcell.00164.2012.

29.**Zhu S, Han G, White RE.** PGE2 action in human coronary artery smooth muscle: role of potassium channels and signaling cross-talk. *J Vasc Res* 39(6): 477–88, 2002. doi: 10.1159/000067201.

30.**Ruan YC, Wang Z, Du JY, Zuo WL, Guo JH, Zhang J, Wu ZL, Wong HY, Chung YW, Chan HC, Zhou WL.** Regulation of smooth muscle contractility by the epithelium in rat vas deferens: role of ATP-induced release of PGE2. *J Physiol* 586(20): 4843–57, 2008. doi: 10.1113/jphysiol.2008.154096.

31.**Martinez-Cutillas M, Mañé N, Gallego D, Jimenez M, Martin MT.** EP2 and EP4 receptors mediate PGE2 induced relaxation in murine colonic circular muscle: pharmacological characterization. *Pharmacol Res* 90: 76–86, 2014. doi: 10.1016/j.phrs.2014.10.001.

32.**Kume H, Hall IP, Washabau RJ, Takagi K, Kotlikoff MI.** β-adrenergic agonists regulate KCa channels in airway smooth muscle by cAMP- dependent and -independent mechanisms. *J Clin Invest* 93: 371–379, 1994. doi:10.1172/JCI116969.

33.**Dib-Hajj SD, Cummins TR, Black JA, Waxman SG.** From genes to pain: Na v 1.7 and human pain disorders. *Trends Neurosci* 30(11): 555–63, 2007. doi: 10.1016/j.tins.2007.08.004.

34.**Liu P, Li S, Tang L.** Nerve Growth Factor: A Potential Therapeutic Target for Lung Diseases. *Int J Mol Sci* 22(17): 9112, 2021. doi: 10.3390/ijms22179112.

35.**Nassenstein C, Schulte-Herbrüggen O, Renz H, Braun A.** Nerve growth factor: the central hub in the development of allergic asthma? *Eur J Pharmacol* 533(1-3): 195–206, 2006. doi: 10.1016/j.ejphar.2005.12.061.

36.**Freund-Michel V, Frossard N.** The nerve growth factor and its receptors in airway inflammatory diseases. *Pharmacol Ther* 117(1): 52–76, 2008. doi: 10.1016/j.pharmthera.2007.07.003.

37.**Stabile A, Pistilli A, Crispoltoni L, Montagnoli C, Tiribuzi R, Casali L, Rende M.** A role for NGF and its receptors TrKA and p75NTR in the progression of COPD. *Biol Chem* 397(2): 157–63, 2016. doi: 10.1515/hsz-2015-0208.

38.**Freund V, Pons F, Joly V, Mathieu E, Martinet N, Frossard N.** Upregulation of nerve growth factor expression by human airway smooth muscle cells in inflammatory conditions. *Eur Respir J* 20(2): 458–63, 2002. doi: 10.1183/09031936.02.00269202.

39. **Kocmalova M, Kazimierova I, Barborikova J, Joskova M, Franova S, Sutovska M.** The Changes in Expression of $Na_V1.7$ and $Na_V1.8$ and the Effects of the Inhalation of Their Blockers in Healthy and Ovalbumin-Sensitized Guinea Pig Airways. *Membranes (Basel)* 11(7): 511, 2021. doi: 10.3390/membranes11070511.

Figure Legends

Fig. 1. *A*: current obtained from a freshly isolated ASMC evoked by stepping from -100 mV to -20 mV in the presence of $[Na^+]_o$ = 130 mM and 13 mM (male). *B*: summary of effect of reducing $[Na^+]_o$ (*n* = 6, 2 female & 4 male, *t*-test). *C*: representative currents from an ASMC evoked by stepping from -100 mV to -30, -20, -10, and 0 mV (female). *D*: summary *I-V* relationship in ASMCs (*n*=18, 7 female & 11 male). *E*: representative currents from an ASMC evoked by stepping from different conditioning potentials to a test potential of -20 mV (female). The conditioning potential preceding each sweep is indicated (-120 to -40 mV). *F*: mean steady-state inactivation curve (o) for ASMCs (*n* = 18, 9 female & 9 male) and activation curve derived from data in Fig. 1*D* (•). Solid lines are fits obtained from the Boltzmann equation. G/G_{max}, normalized conductance.

Fig. 2. *A, B* and *C*: primers for $Na_V1.1$-1.9 were tested in mouse brain (male), bronchus (female) and ASMCs (three examples of ASMCs from three different mice, refer to Table 1 for breakdown of expression in eight mice). *D*: Non template control (NTC) for reagents used to determine Na_V expression. *E* (female) and *F* (female): primers for smooth muscle myosin heavy chain (MHC, smooth muscle cell marker), ubiquitin carboxy-terminal hydrolase L1 (UCH-L1, neuronal cell marker), carboxypeptidase A3 (CarbA3, mast cell marker) and prolyl 4-hydroxylases (P4H, fibroblast marker) were tested in brain and ASMCs. ASMC samples which expressed only MHC were tested for Na_V expression. Amplicons were resolved on an agarose gel (2%) and visualized using SYBR Safe.

Table 1. Expression of m RNA Na_V channel subtypes in isolated ASMC. ASMCs expressed $Na_V1.7$ in 7 out of 8 samples. The transcriptional expression of $Na_V1.6$ was observed in 4 out of 8 samples. Expression of $Na_V1.2$ and $Na_V1.9$ was positive in 3 out of 8 samples. Both $Na_V1.1$ and $Na_V1.5$ were expressed in 1 out of 8 samples.

Fig. 3. A: effect of TTX on an isolated ASMC (M). B: concentration-effect relationship for TTX in ASMCs (*n* = 8, 5 female & 3 male). *C*: effect of PF-05089771 on an isolated ASMC (F). *D*: concentration-effect relationship for PF-05089771 in ASMCs (*n* = 7, 2 female & 5 male). *E*: effect of 4,9,-anhydro-TTX (10 nM - 1 μM) on an isolated ASMC (female). *F*: concentration-effect relationship for 4,9,-anhydro-TTX in ASMCs (*n* = 6, 2 female & 4 male). Currents were evoked by stepping from -100 mV to -20 mV. Solid lines show fits with the Hill-Langmuir equation.

Fig. 4. *A*: effect of OD1 (50 nM) on peak and (*B*) sustained I_{Na} in an isolated ASMC (male). *C*: summary of peak current amplitude, taken within the first 10 ms of the sweep (n = 7, 3 female & 4 male, *t*-test). *D*: summary sustained current amplitude, taken within the last 10 ms of the sweep, before and after exposure to 50 nM OD1 (n = 7, 3 female & 4 male, *t*-test). Currents were evoked by stepping from -100 mV to -20 mV.

Fig. 5. *A:* effect of veratridine (30 μM) and then veratridine + TTX (100 nM) on peak and (*B*) sustained I_{Na} in an isolated ASMC (M). *C*: summary of peak current amplitude, taken in the first 10 ms of the sweep and (*D*) sustained current amplitude, taken in the last 10 ms of the sweep (n = 6, 1 female & 5 male). Currents were evoked by stepping from -100 mV to -20 mV. P values obtained using ANOVA and Tukey's *post hoc* test.

Fig. 6. *A*: representative tension recording demonstrating the effect of veratridine (10 μM) before and after atropine (1 μM), (female). *B*: Summary of effect of veratridine (10 μM) before and after atropine (1 μM), (n = 6; 5 female & 1 male, *t*-test). *C*: representative tension recording demonstrating the effect of U-46619 (100 nM) and PGE_2 (100 nM) on a mouse bronchial ring in the presence of atropine (1 μM), (female). This treatment stimulated a series of oscillations ('bursts'). *D*: representative tension recording demonstrating the effect of veratridine (10 μM), then TTX (100 nM) on 'bursts', (M). *E*: summary of effect of veratridine (10 μM), then TTX (100 nM) on 'burst' duration (n = 6, 1 female & 5 male, Wilcoxin test, 'bursts' induced as in *C*). *F*: representative tension recording demonstrating the effect of TTX (100 nM) on 'bursts', (male). *G*: summary of mean 'burst' duration in the presence and absence of TTX (n = 10, 2 female & 8 male, *t*-test, 'bursts' induced as in *C*).

Fig. 7. *A*: immunofluorescent detection of Na_V in isolated ASMCs. ASMCs were treated with an anti-Pan Na_V primary antibody (1:200) and donkey anti-goat Alexa Fluor-488 conjugation secondary antibody (1:1000, n = 3). *B*: immunofluorescent detection of SCN9A in isolated ASMCs. ASMCs were treated with an anti-SCN9A primary antibody (intracellular epitope, 1:200) and donkey anti-goat Alexa Fluor-488 conjugated secondary antibody (1:1000; n = 3). *C*: immunofluorescent detection of SCN9A in isolated ASMCs. ASMCs were treated with an anti-SCN9A primary antibody (extracellular epitope, 1:100) and donkey anti-goat Alexa Fluor-488 conjugated secondary antibody (1:1000; n = 3).

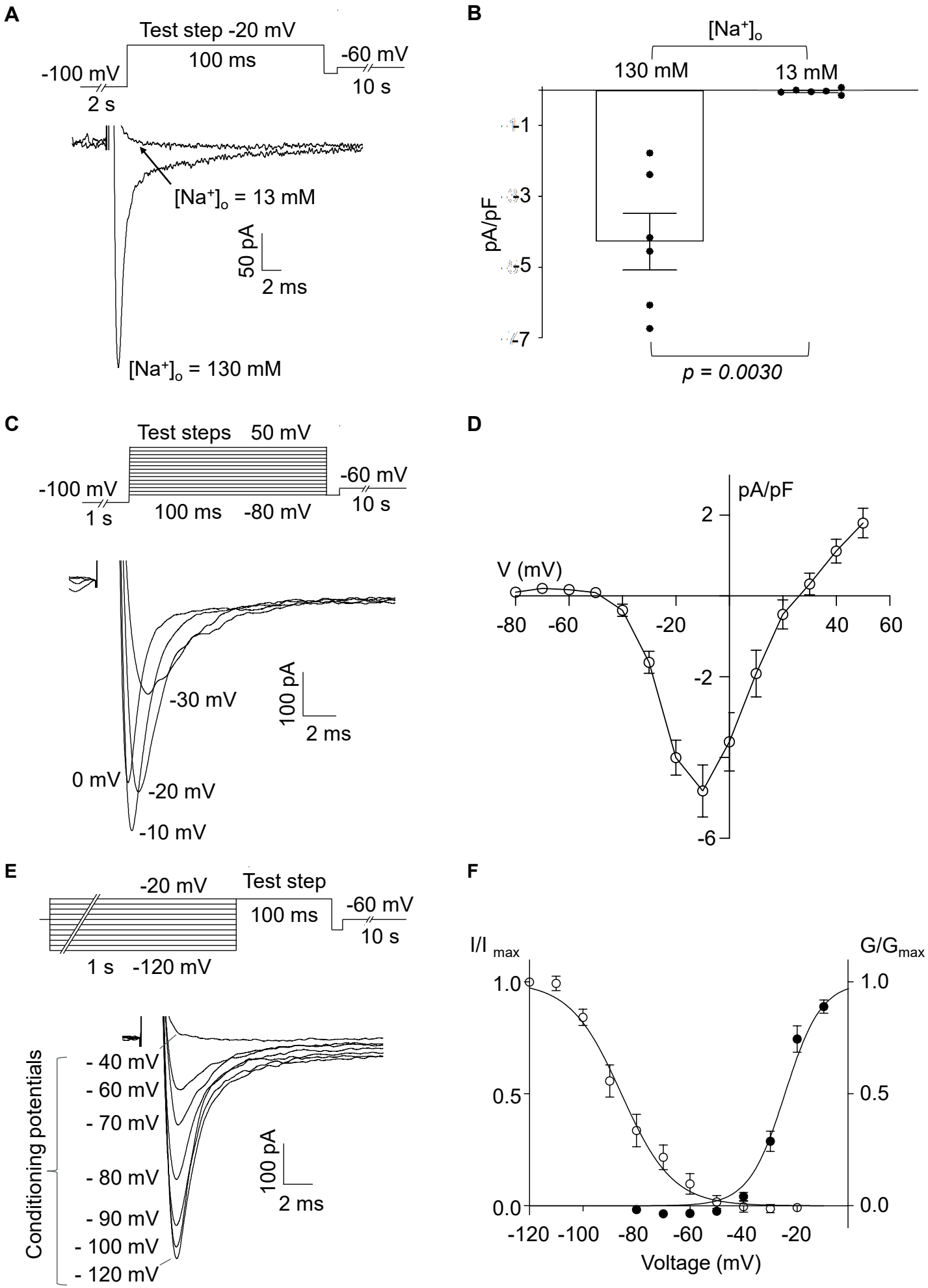
A
Test step -20 mV
100 ms
-60 mV
-100 mV
10 s
2 s
[Na+]o = 13 mM
50 pA
2 ms
[Na+]o = 130 mM
B
[Na+]o
130 mM
13 mM
-1
-3
-5
-7
pA/pF
p = 0.0030
C
Test steps 50 mV
-60 mV
-100 mV
10 s
1 s
100 ms -80 mV
-30 mV
100 pA
2 ms
0 mV
-20 mV
-10 mV
D
pA/pF
2
V (mV)
-80 -60 -20 40 60
-2
-6
E
-20 mV
Test step
100 ms
-60 mV
10 s
1 s -120 mV
Conditioning potentials
- 40 mV
- 60 mV
- 70 mV
- 80 mV
- 90 mV
- 100 mV
- 120 mV
100 pA
2 ms
F
I/I max
G/Gmax
1.0
0.5
0.0
-120 -100 -80 -60 -40 -20
Voltage (mV)

Fig. 1

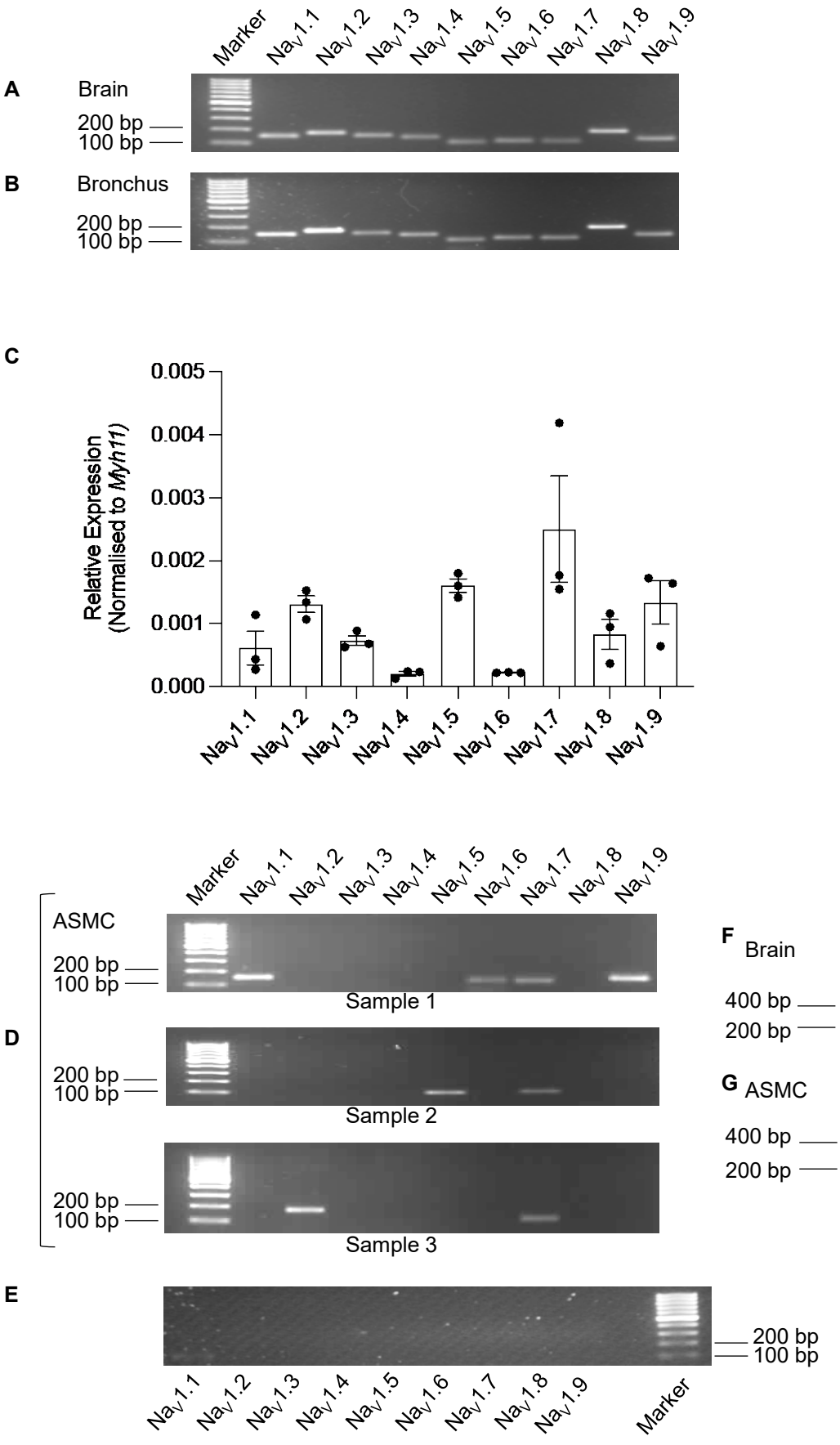
A
Brain
200 bp
100 bp
Marker
NaV1.1
NaV1.2
NaV1.3
NaV1.4
NaV1.5
NaV1.6
NaV1.7
NaV1.8
NaV1.9
B
Bronchus
200 bp
100 bp
C
Relative Expression
(Normalised to Myh11)
0.005
0.004
0.003
0.002
0.001
0.000
D
ASMC
200 bp
100 bp
Sample 1
Sample 2
Sample 3
E
200 bp
100 bp
F
Brain
400 bp
200 bp
Marker
MHC
UCH-L1
CarbA3
P4H
G
ASMC
400 bp
200 bp

Fig. 2

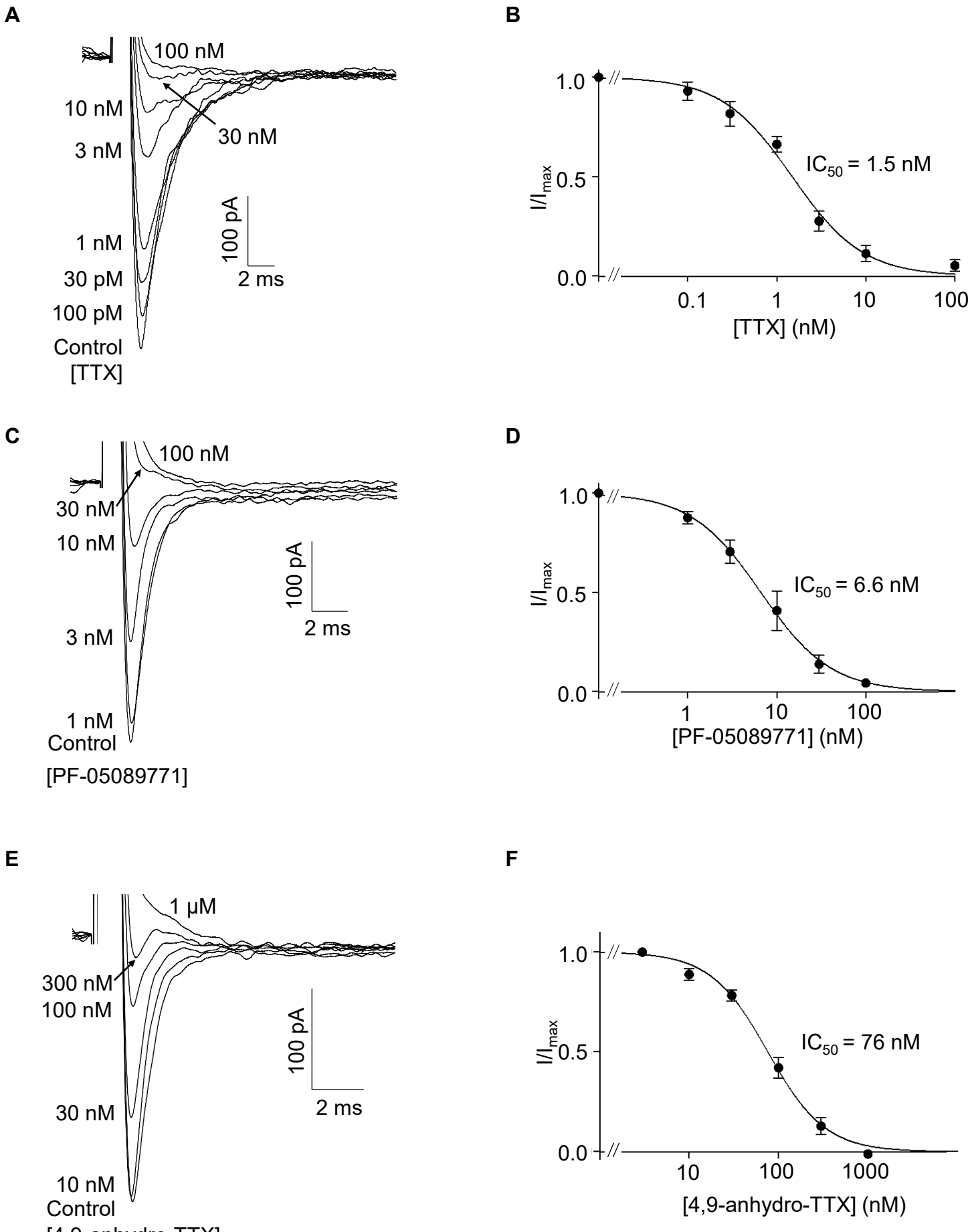
A
100 nM
10 nM
30 nM
3 nM
100 pA
2 ms
1 nM
30 pM
100 pM
Control
[TTX]
B
1.0
0.5
0.0
I/I_max
IC50 = 1.5 nM
0.1
1
10
100
[TTX] (nM)
C
100 nM
30 nM
10 nM
100 pA
2 ms
3 nM
1 nM
Control
[PF-05089771]
D
1.0
0.5
0.0
I/I_max
IC50 = 6.6 nM
1
10
100
[PF-05089771] (nM)
E
1 µM
300 nM
100 nM
100 pA
2 ms
30 nM
10 nM
Control
[4,9-anhydro-TTX]
F
1.0
0.5
0.0
I/I_max
IC50 = 76 nM
10
100
1000
[4,9-anhydro-TTX] (nM)

Fig. 3

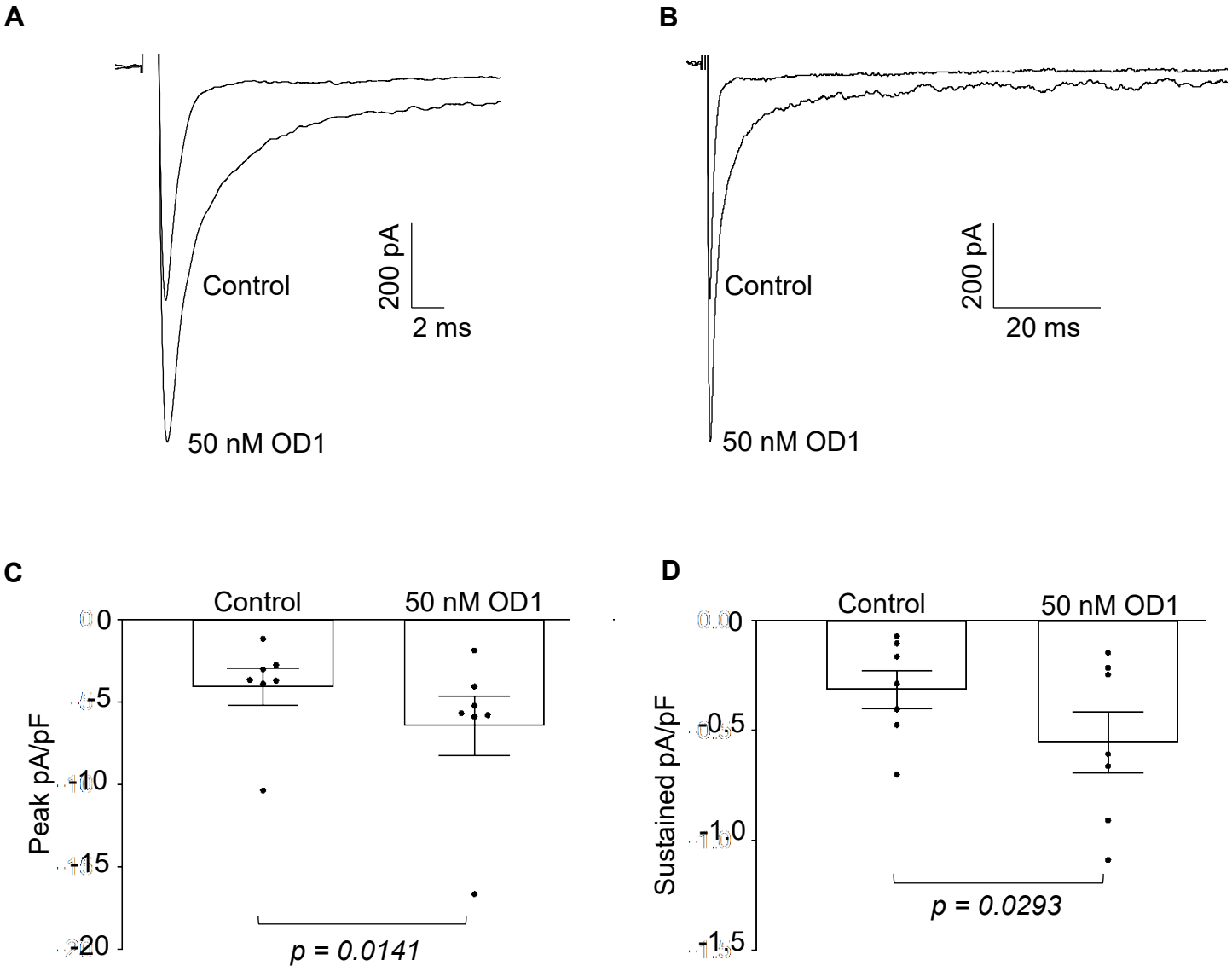
A
Control
200 pA
2 ms
50 nM OD1
B
Control
200 pA
20 ms
50 nM OD1
C
Control
50 nM OD1
Peak pA/pF
0
-5
-10
-15
-20
p = 0.0141
D
Control
50 nM OD1
Sustained pA/pF
0.0
-0.5
-1.0
-1.5
p = 0.0293

Fig. 4

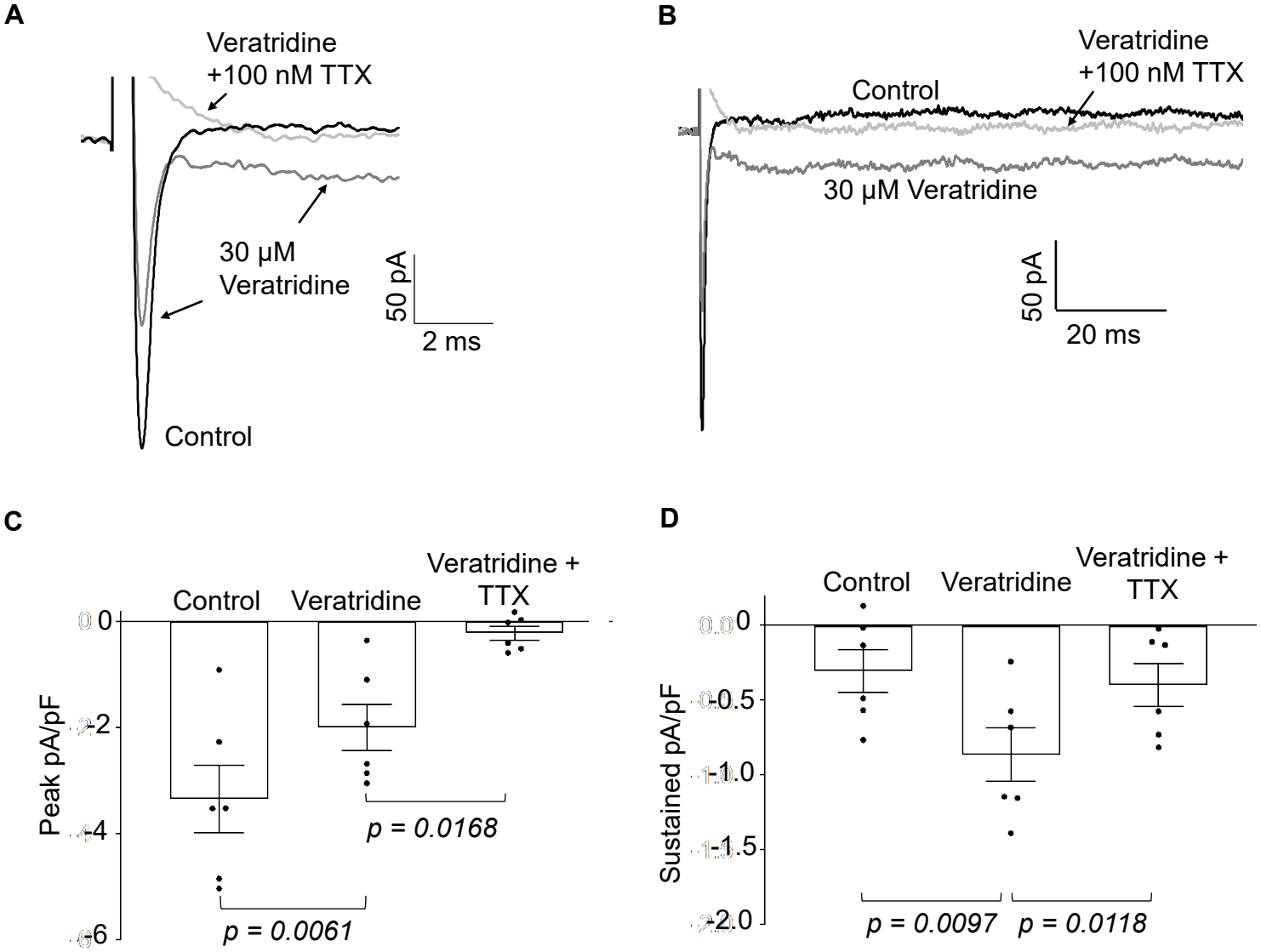
A
Veratridine
+100 nM TTX
30 μM
Veratridine
50 pA
2 ms
Control
B
Veratridine
+100 nM TTX
Control
30 μM Veratridine
50 pA
20 ms
C
Control
Veratridine
Veratridine +
TTX
Peak pA/pF
0
-2
-4
-6
p = 0.0168
p = 0.0061
D
Control
Veratridine
Veratridine +
TTX
Sustained pA/pF
0.0
-0.5
-1.0
-1.5
-2.0
p = 0.0097
p = 0.0118

Fig. 5

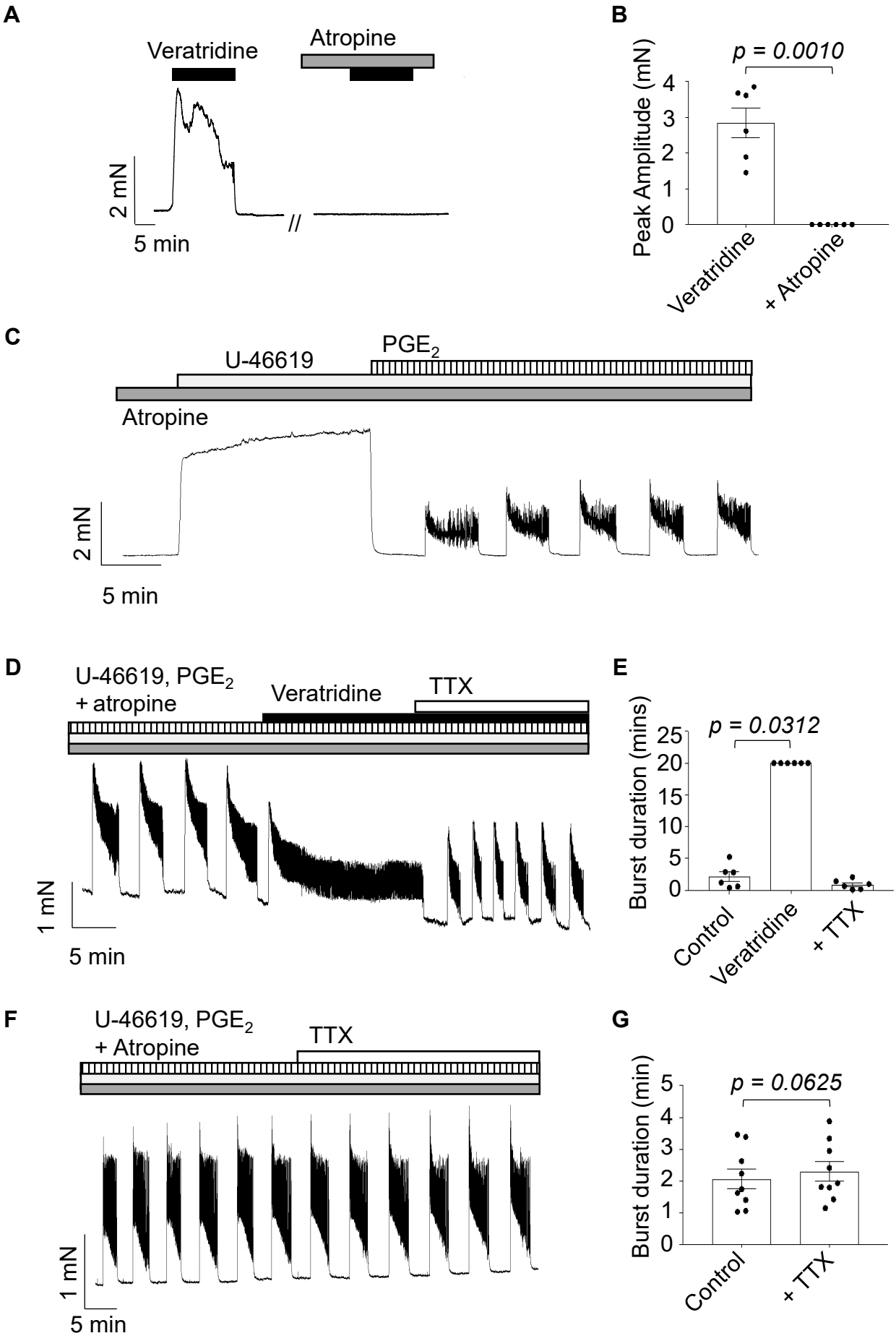
A
Veratridine
Atropine
2 mN
5 min
//
B
p = 0.0010
Peak Amplitude (mN)
0
1
2
3
4
Veratridine
+ Atropine
C
U-46619
PGE2
Atropine
2 mN
5 min
D
U-46619, PGE2
+ atropine
Veratridine
TTX
1 mN
5 min
E
p = 0.0312
Burst duration (mins)
0
5
10
15
20
25
Control
Veratridine
+ TTX
F
U-46619, PGE2
+ Atropine
TTX
1 mN
5 min
G
p = 0.0625
Burst duration (min)
0
1
2
3
4
5
Control
+ TTX

Fig. 6

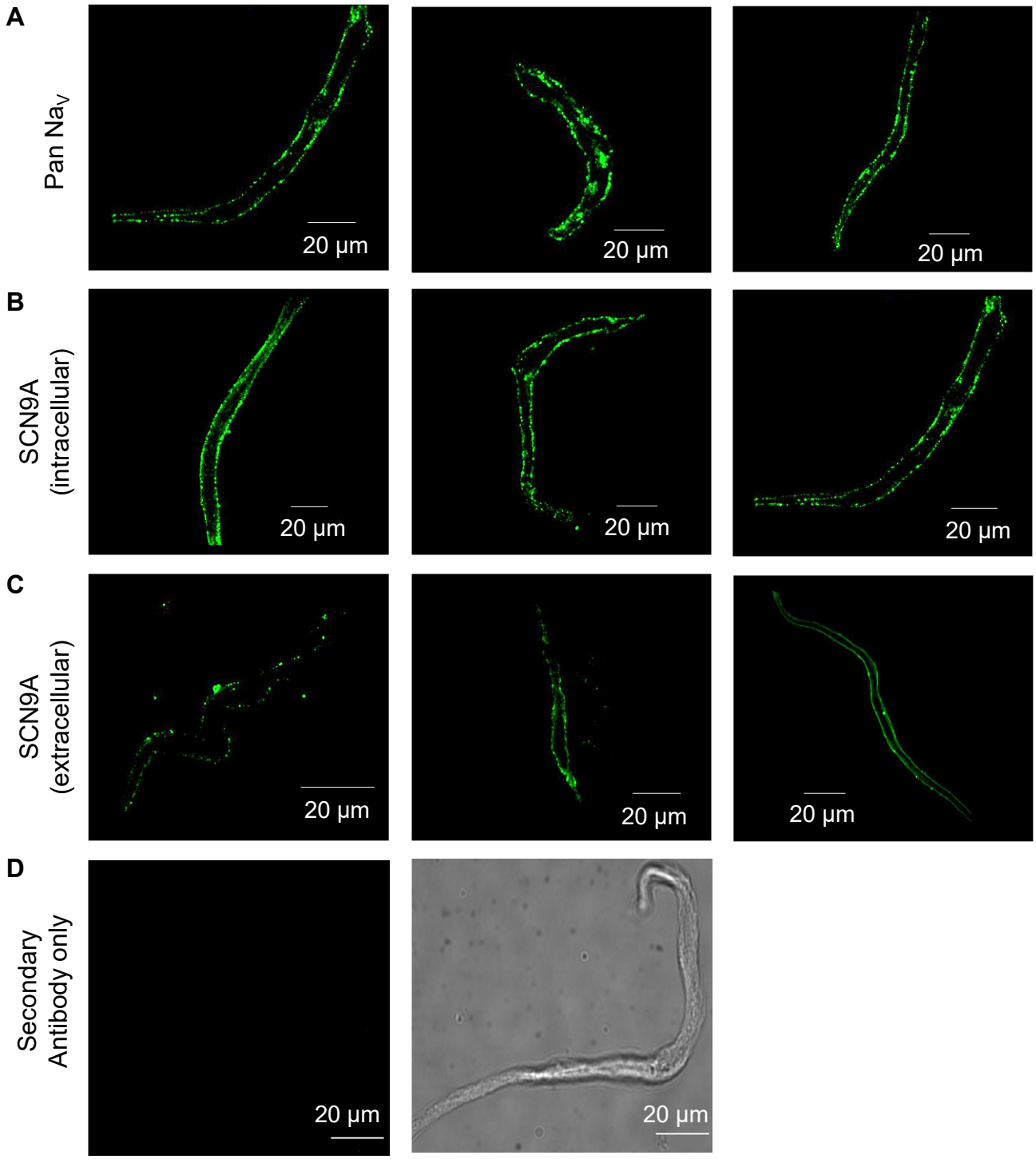
A
Pan Na_V
20 µm
20 µm
20 µm
B
SCN9A
(intracellular)
20 µm
20 µm
20 µm
C
SCN9A
(extracellular)
20 µm
20 µm
20 µm
D
Secondary
Antibody only
20 µm
20 µm

Fig. 7

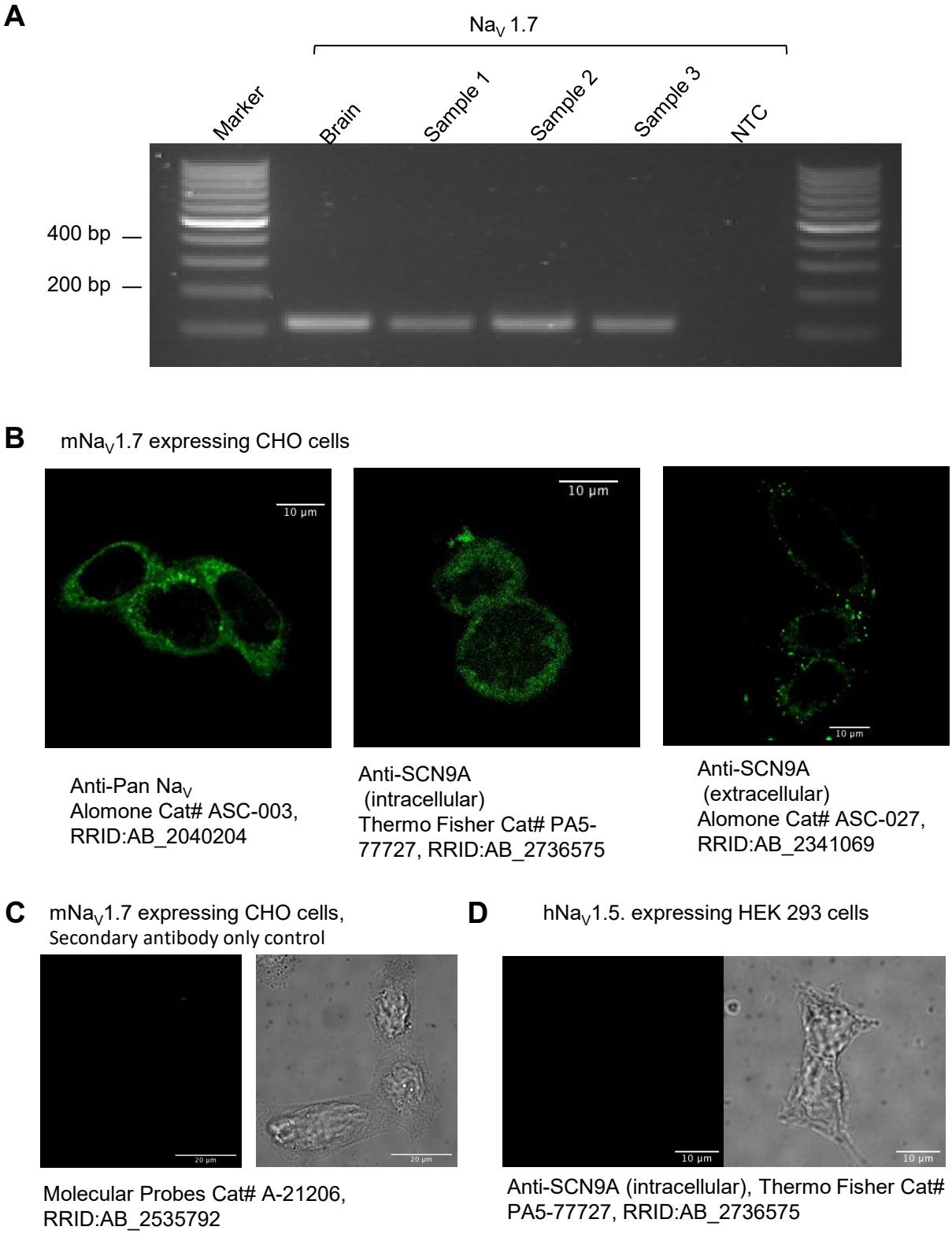

Fig. S1. Validation of expression of the Na$_V$1.7 α-subunit in Na$_V$1.7-CHO cells. *A:* RT-PCR expression of Na$_V$1.7 confirming a positive gene expression profile in this cell line. Sample 1, 2 and 3 represent three experiment repetitions (n=3). NTC = non template control. Amplicons were resolved on an agarose gel (2%) and visualised using SYBR Safe. *B*: Immunological detection of Na$_V$ protein in CHO expressing mNa$_V$1.7. Scale bars 10 µm. *C*: Secondary antibody only control. Scale bars 20 µm. *D*: Anti-SCN9A (intracellular, RRID:AB_2736575) did not cross react with human Na$_V$1.5, expressed in HEK 293 cells. Scale bars 10 µm.

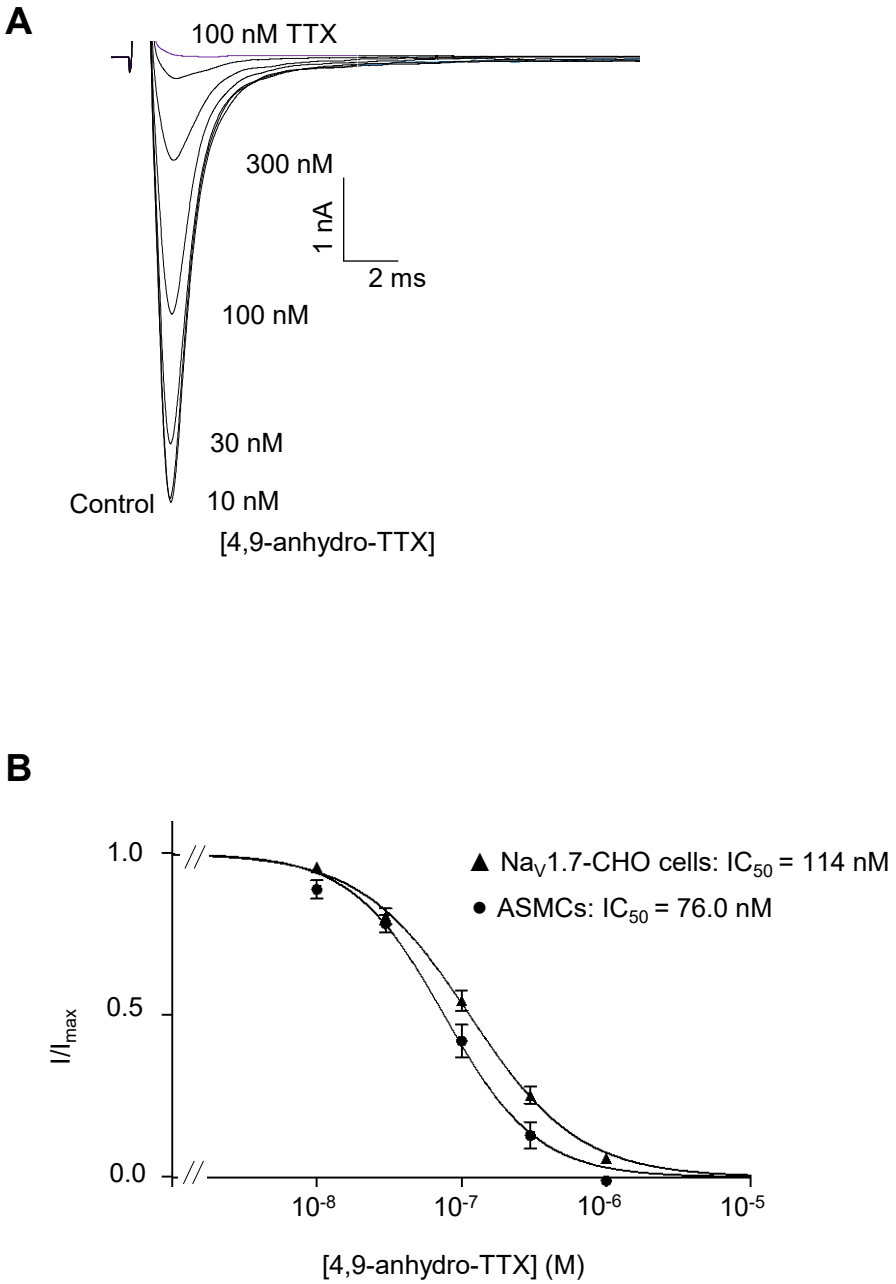

Fig. S2. Concentration dependent effect of 4,9-anhydro-TTX on mNa$_V$1.7-CHO cells. *A*: Effect of 4,9-anhydro-TTX (10 nM – 1 μM) on mNa$_V$1.7-CHO cells. Currents were evoked by stepping from -140 mV to -10 mV. *B*: Concentration-effect relationship for 4,9-anhydro-TTX in mNa$_V$1.7-CHO cells (▲, *n*=9) and ASMCs (●, data derived from Fig. 3F). Solid lines shows fit with the Hill-Langmuir equation.

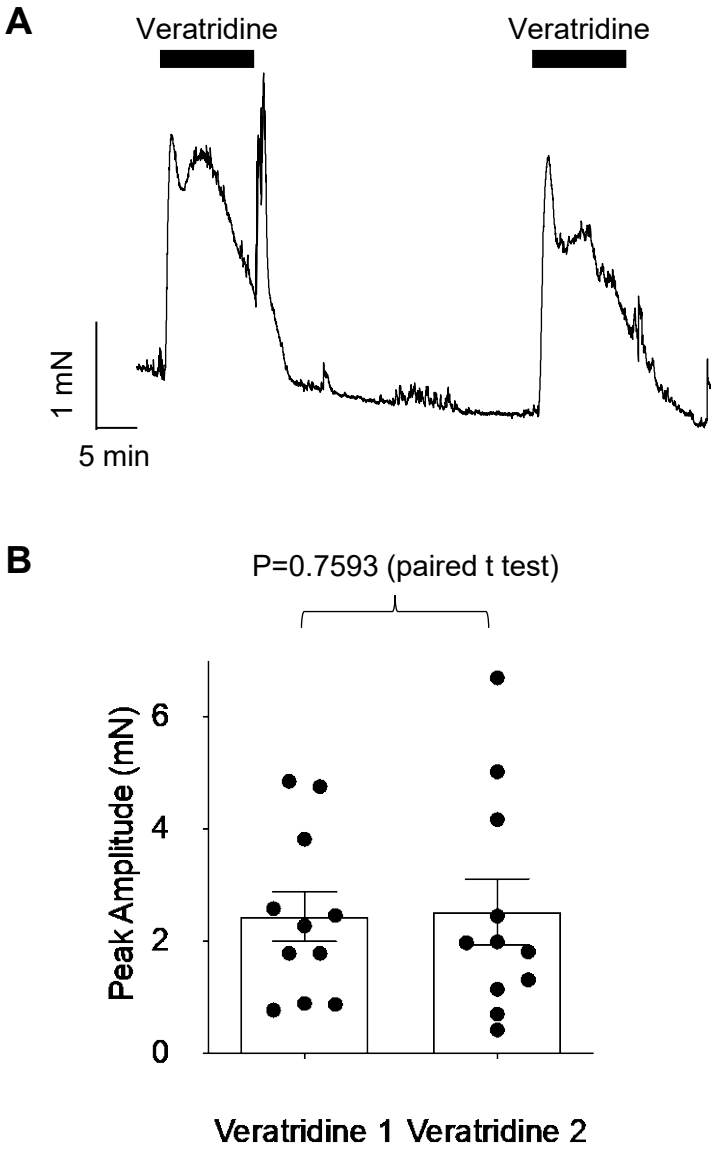

Fig. S3. Time control for veratridine tension experiments. *A*: Representative trace of the the effect of applying veratridine (10 μM) on two occasions. The late spike in the first response is a washout artifact. *B*: Summary of 11 similar experiments as in *A*. There was no significant difference between the responses.

Table S1

Primer Name	Genbank ID	Sequence (5'-3')	Amplicon Size (bp)
$Na_V1.1$ F	NM_018733.2	AACAAGCTTCATTCACATACAATAAG	150
$Na_V1.1$ R		AGGAGGGCGGACAAGCTG	
$Na_V1.2$ F	NM_001346680.1	ATTTTCGGCTCATTCTTCACACT	176
$Na_V1.2$ R		GGGCGAGGTATCGGTTTTTGT	
$Na_V1.3$ F	NM_018732.3	CAGACCATGTGCCTTATTGTGT	154
$Na_V1.3$ R		CCGCGATCTGGAGGTTGTT	
$Na_V1.4$ F	NM_133199.2	AGTCCCTGGCAGCCATAGAA	140
$Na_V1.4$ R		CCCATAGATGAGTGGGAGGTT	
$Na_V1.5$ F	NM_001253860.1	ATGGCAAACTTCCTGTTACCTC	104
$Na_V1.5$ R		CCACGGGCTTGTTTTTCAGC	
$Na_V1.6$ F	NM_011323.3	GCAAGCTCAAGAAACCACCC	115
$Na_V1.6$ R		CCGTAGATGAAAGGCAAACTCT	
$Na_V1.7$ F	NM_001290674.1	TGGATTCCCTTCGTTCACAGA	115
$Na_V1.7$ R		GTCGCAGATACATCCTCTTGTTT	
$Na_V1.8$ F	NM_009134.3	TCCGTGGGAACTACCAACTTC	190
$Na_V1.8$ R		GCTCGCCATAGAACCTGGG	
$Na_V1.9$ F	NM_011887.3	CGACTCTTTGGCTGCAATAGA	134
$Na_V1.9$ R		AGAGCTTAGGTAACTTCCTGGAG	
SMM F	NM_013607.2	TACAAGGAGCAGGCAGAGAA	
SMM R		GCTCACTGCGAAGTTTCCT	218
UCH-L1 F	NM_011670.2	GGAGATTAACCCCGAGATGC	252
UCH-L1 R		CAGGAGTTTCCGATGGTCTG	
CarbA3 F	NM_007753.2	AGGCTCTTCCTTAGACTGGG	226
CarbA3 R		GACTCCACCAAGCATTGAT	
P4H F	NM_011030.2	GGAGCCTTGGAGACGGTA	266
P4H R		TCGCTCATATAGAACAGCCAC	